Anharmonicity and disorder on the Cu(110) surface

P. D. Ditlevsen, P. Stoltze, and J. K. Nørskov
Laboratory of Applied Physics, Technical University of Denmark, DK-2800 Lyngby, Denmark
(Received 26 April 1991)

The results of a molecular-dynamics simulation of the finite-temperature properties of the Cu(110) surface are presented. The interatomic interactions have been calculated using the effective-medium theory. The temperature dependence of the interlayer spacings, phonon frequencies and lifetimes, and the structure factor is calculated. The anharmonic effects are shown to be considerably stronger than in the bulk, giving rise to a large thermal expansion coefficient and to a phonon density of states with large peak shifts and widths, in good agreement with experiment. Anharmonicity is also shown to be responsible to the loss of order above 550 K observed in a number of scattering experiments. Above 1000 K an additional loss of order sets in. Here the in-plane order disappears due to rearrangements of the surface atoms around the adatoms and vacancies that are formed at these temperatures. As the temperature is increased further toward the melting point, the disorder moves deeper into the crystal.

I. INTRODUCTION

The finite-temperature properties of metal surfaces differ substantially from those of the bulk. The thermal expansion coefficient for the first interlayer spacing at the surface is much larger than in the bulk.[1] A roughening transition has been reported on several surfaces,[2] and another disordered state with properties that are meltlike is found in some cases at temperatures well below the melting point.[3] The surface phonons have also been found to shift and broaden significantly more than in the bulk[4] when the temperature is increased.

On the Cu(110) surface a significant change in the behavior has been reported in the region around 550 K. At temperatures higher than that, the He scattering,[5,6] photoemission,[7] low-energy ion scattering,[8] inverse photoemission,[8] and x-ray scattering intensities[9] decrease significantly faster than predicted by a simple Debye-Waller factor. The strong attenuation of the scattering above 550 K has been attributed to a roughening transition,[5,9] but this has been ruled out by Zeppenfeld *et al.*[6] in a study of the angular profiles in elastic He scattering. Zeppenfeld *et al.*[6] point to the importance of anharmonicity in the vibrations at the surface as the main source of the decrease in scattering intensity above 550 K. Direct measurements of the surface phonons as a function of temperature clearly show a substantial temperature-induced shift and broadening of the electron-energy-loss (EELS) peaks arising from phonon modes localized at the surface,[4] thus supporting the notion that surface anharmonicity is important. This was also inferred from the low-energy ion scattering and inverse photoemission experiments,[8] but these experiments also showed that a substantial number of adatom-vacancy pairs are present at the surface at these temperatures.

A theoretical discussion of the disordering of Cu surfaces within the quasiharmonic approximation has been presented by Jayanthi, Tosatti, and Pietronero.[10] In the present paper we present a molecular-dynamics simulation of Cu(110) at temperatures up to 1600 K with our aim being to contribute to the understanding of the relative role of the various effects on the surface. We show that the simulation can reproduce the measured temperature-induced effects in the phonon spectra and the change in scattering properties above 550 K. The simulations clearly show that surface anharmonicity is responsible for these effects, and we are able to analyze the origin of the strong anharmonicity at the surface. At higher temperatures adatom-vacancy pairs are formed and at a temperature around 1000 K we observe a strong increase in the disorder which we ascribe to premelting induced by the adatom-vacancy pair formation.

In the following we first briefly describe the computational method. In the next sections we then describe the calculation of the thermal expansion at the surface and the finite-temperature phonon spectra. We then go on to the calculation of the structure factor, which allows us to discuss the role of anharmonicity and other sources of disorder in scattering and diffraction experiments. In the section following that we discuss the role of adatoms and vacancies formed at the surface at elevated temperatures, and then go on to investigate the order at the highest temperatures including premelting. Finally, we summarize the findings and conclude in the last section.

II. THE CALCULATIONAL METHOD

The effective-medium theory has been used to calculate the interatomic interactions. The expression for the total energy is derived from density-functional theory. It includes in an approximate way the many-body interactions that are essential for a proper description of a metal. For the present purposes it is important to note that the method has been shown to give a good description of the surface energy,[11] interlayer relaxations,[12] adsorbate-

induced reconstructions,[12] and the surface phonons at low temperature[13] (where anharmonic effects are not important) of various copper surfaces. A complete account of the method and the parameters used can be found in Refs. 14 and 13. It is worth noting that all input parameters except one are obtained from local-density calculations of Cu embedded in a homogeneous electron gas. One of the parameters is determined from the measured value of the elastic constant C_{44}. It could also be obtained from other bulk metal properties such as the zone boundary phonon frequencies, but this makes only a tiny difference in the results.[13] The calculational method thus contains no input about the surface or the finite-temperature properties of the system.

The integration of the classical equations of motion for the nuclei is made by the Velocity Verlet algorithm, the elementary time step being 3.4 fs. Each trajectory is a sequence $(\mathbf{r}_i(t_1), \mathbf{r}_i(t_2), \ldots, \mathbf{r}_i(t_N), i \in N_{\text{atom}})$ of the coordinates for all atoms in the system and contains either $N=1500$ configurations at 10.1-fs intervals or $N=300$ configurations at 33.6-fs intervals. The high sampling frequency results in the collection of several configurations per lattice vibration, and is used for the calculation of vibrational spectra. The low sampling frequency is used for the calculations of all other data.

Periods of stochastic thermalization have been alternated with collection of data. This was continued until averages of energy and structure factors were constant in each simulation and reproducible from one trajectory to the next. Given a set of observations, the thermal averages are calculated as time averages as

$$\langle A(T) \rangle = \frac{1}{T} \sum_{i=1}^{N} A(t_i) \tag{1}$$

with $T = t_N - t_1$ being the total sampling period. Simulations have been made at 93-K intervals from 93 to 1670 K. The classical description of the atomic motion limits the reliability of the results at temperatures below 300–400 K, where quantum effects are expected to be important.

The geometry of the computational cell is the following. Eight layers of (110) planes are allowed to move on top of a static substrate. Periodic boundary conditions are applied parallel to the surface, each layer in the surface supercell having 96 (16×6) atoms. The dynamic atoms thus move on a semi-infinite crystal. The static substrate is given a lattice constant which is temperature dependent. The bulk thermal expansion coefficient is determined in an independent calculation (with three-dimensional periodic boundary conditions). This will give a good description of the dynamics in the first layers, which is what we will be interested in here, but for the layers closest to the static substrate the motion will be severely influenced by the static boundary condition.

III. THERMAL EXPANSION

One of the indicators that a purely harmonic description of the motion of the atoms in a solid is not valid is the observation that the lattice constant increases with temperature. Before going into the question of the thermal expansion at the surface, it may be appropriate to mention that a calculation of the thermal expansion coefficient α_{bulk} for bulk Cu using the effective-medium theory for the interatomic interactions gives $\alpha_{\text{bulk}} = 14 \times 10^{-6}$ K^{-1} in good agreement with the experimental value of 17×10^{-6} K^{-1}.[15]

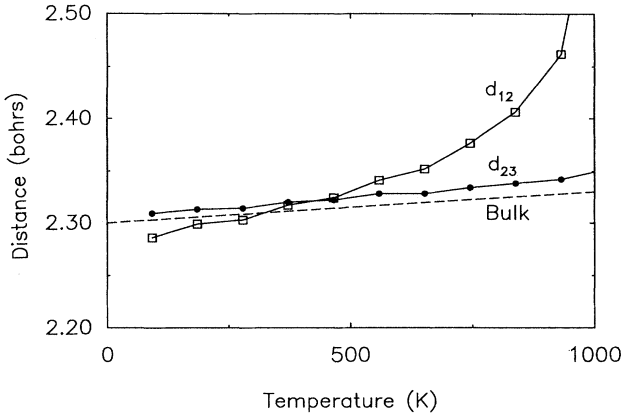

FIG. 1. The thermally averaged interlayer spacings d_{12} (open squares) and d_{23} (circles) for a Cu(110) surface shown as a function of temperature. The bulk thermal expansion is included (dashed) for comparison. Note that the low-temperature (less than 300–400 K) variations must be taken with some caution since quantum effects may be important here.

At the surface the change in interatomic distances will be different perpendicular and parallel to the surface. Parallel to the surface the lattice constant will be determined by the bulk, but perpendicular to the surface a larger anharmonicity at the surface than in the bulk should reveal itself as a larger thermal expansion coefficient. Figure 1 shows the thermally averaged interlayer spacings d_{12} and d_{23} between the first and second and

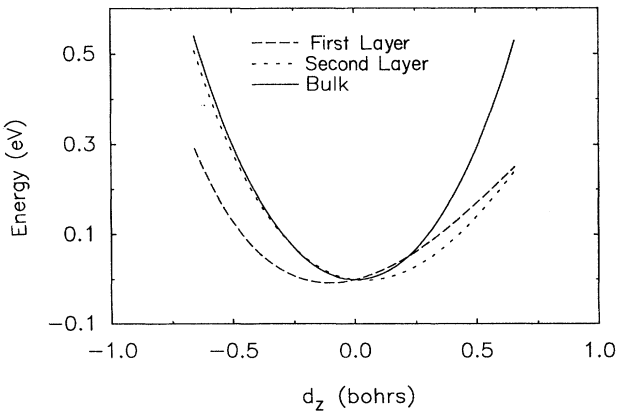

FIG. 2. The calculated potential felt by an atom in the first and second layer on a Cu(110) surface when it is moved perpendicular to the surface. The equivalent potential felt by a bulk atom is shown for comparison.

second and third layers. Clearly, the expansion is considerably larger at the surface than in the bulk. At the lowest temperatures the temperature dependence of d_{12} is approximately linear with a thermal expansion coefficient approximately a factor of 3 larger than for the deeper layers and the bulk. At higher temperatures the interlayer spacing starts to increase drastically both due to anharmonic effects and because adatoms are being formed which contribute significantly to the average interlayer spacing. This behavior is very similar to that observed experimentally for Pb(110).[1]

The large thermal expansion at the surface compared to the bulk is not surprising when one considers the potential that a first- or second-layer atom on the (110) surface experiences when it is moved perpendicular to the surface in Fig. 2. Clearly both the first- and (to a lesser extent) second-layer atoms feel a very anharmonic potential. The potential felt by a bulk atom is included for reference, and the difference to the surface behavior is striking. The large anharmonicity at the surface mainly stems from the fact that both the first- and second-layer atoms have lost nearest neighbors compared to the bulk.

IV. TEMPERATURE DEPENDENCE OF THE SURFACE PHONONS

The anharmonic effects at the surface can be further studied by considering the temperature dependence of the phonon spectrum. We do this by calculating the momentum autocorrelation function in layer l along the direction α as[16]

$$n_l^\alpha(\mathbf{k},\omega) = \int \frac{dt}{2\pi} e^{-i\omega t} n_l^\alpha(\mathbf{k},t), \tag{2}$$

where

$$n_l^\alpha(\mathbf{k},t) = \frac{\langle p_{l,\mathbf{k}}^\alpha(0) p_{l,\mathbf{k}}^\alpha(t)\rangle}{\sum_{m,\beta}\langle p_{m,\mathbf{k}}^\beta(0) p_{m,\mathbf{k}}^\beta(0)\rangle/3N_{\text{layer}}} \tag{3}$$

and

$$p_{l,\mathbf{k}}^\alpha(t) = \frac{1}{N_l}\sum_{i\in l} p_i^\alpha(t) e^{-i\mathbf{k}\cdot\mathbf{R}_i(t)}. \tag{4}$$

Here $\mathbf{k}$ is a wave vector in the surface plane, and the sum over atoms i is over the N_l atoms in a particular layer l such that the atom is included in the sum if it is less than half an interlayer spacing away from the layer. The index $\alpha = x, y$, or z on the instantaneous momentum $\mathbf{p}_i(t)$ of atom i indicates that only the motion in the α direction is considered. N_{layer} is the number of layers. In the Appendix we show that $n_l^\alpha(\mathbf{k},\omega)$ is equal to the phonon density of states in layer l along the direction α in the harmonic approximation.

The correlation function $n_l^\alpha(\mathbf{k},\omega)$ can be expressed directly in terms of the Fourier transform

$$p_{l,\mathbf{k}}^\alpha(w) = \int \frac{dt}{2\pi} e^{-i\omega t} p_{l,\mathbf{k}}^\alpha(t) \tag{5}$$

as

$$n_l^\alpha(\mathbf{k},\omega) = \frac{1}{\langle p_{\mathbf{k}}^2\rangle}|p_{l,\mathbf{k}}^\alpha(\omega)|^2, \tag{6}$$

where $\langle p_{\mathbf{k}}^2\rangle$ is shorthand for the denominator in Eq. (3).

We calculate the power spectrum $p_{l,\mathbf{k}}^\alpha(w)$ from a discrete series of $p_{l,\mathbf{k}}^\alpha(t)$ sampled during the simulation using Burg's algorithm.[17]

To illustrate the influence of anharmonicity on the vibrational spectrum of Cu(110) we will concentrate on the three zone boundary states at $\bar{Y}$ that are split off below the bulk phonon bands. They are all gap states that are localized at the surface and we therefore do not have any problems with the finite thickness of the computational box in the calculation. The motion of the atoms in the outermost layers is illustrated in Fig. 3.

In Table I we compare the frequencies obtained for these three modes in the present calculation (at 100 K) with the result of a simpler calculation within the harmonic approximation[13] and with experiment.[18] The agreement between the two calculations and with experiment is seen to be good. For the S_1 mode the present calculation is closer to the experiment than is the harmonic one. This is not due to anharmonic effects at the low temperature considered. Rather the difference can be traced back to a difference in the range of the electron density contributions that were included in the total energy calculation. In the harmonic calculation only nearest-neighbor contributions have been included, whereas in the molecular-dynamics simulation contributions from up

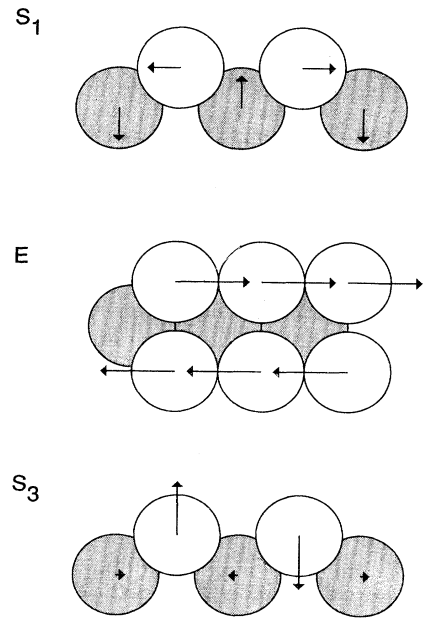

FIG. 3. Schematic illustration of the motion of the two outermost layers for the three $\bar{Y}$ zone boundary phonons on the Cu(110) surface. The polarizations in different directions and in the first few layers as calculated in the harmonic approximation are indicated by the lengths of the vectors shown.

TABLE I. The low-temperature (100 K) phonon frequencies of the three $\bar{Y}$ modes S_1, E, and S_3 that are split below the bulk phonon bands on the Cu(110) surface. The result of the present calculation is compared to that of a harmonic treatment with only nearest-neighbor density contributions included (Ref. 13) and to experiment (Ref. 18). The experimental value shown for the S_1 mode is extrapolated from the published spectra (Ref. 18). Frequencies are in meV.

	Simulation	Harmonic model	Experiment
S_1	8.1	10.4	7.3
E	11.4	11.7	
S_3	13.0	13.0	12.4

to third-nearest neighbors have been included in the electron density sums. This results in slight changes in the second-, third-, and fourth-nearest-neighbor interactions. For most modes this makes only a small difference, but in the S_1 mode the surface atoms are moving directly toward the second-nearest neighbors (cf. Fig. 3) in the surface plane, which means that the second-nearest-neighbor effects are largest here.

The calculated spectrum projected onto the first layer is shown in Fig. 4 for two different temperatures. It is clearly seen how the peaks shift and broaden when the temperature is increased. We characterize the temperature dependence of the phonon peaks found by their first and second moments,

$$\Omega = \int \omega n_l^{\alpha}(\mathbf{k},\omega)d\omega, \tag{7}$$

$$\Delta = \int (\omega - \Omega)^2 n_l^{\alpha}(\mathbf{k},\omega)d\omega, \tag{8}$$

giving the peak position and width, respectively. The moments are calculated from the spectra using a window of width 5 meV around the peak to avoid contributions from other peaks in the spectrum. The results for $\Omega(T)$ and $\Delta(T)$ for the S_3 mode are shown in Fig. 5 together with the results of an EELS experiment of Baddorf and Plummer[4] which exists for this case. It is seen that both the variation of frequency and the width are in excellent agreement with experiment. The figure also includes the result of a calculation of the frequency shift in the quasiharmonic approximation. This is a purely harmonic calculation where the thermal expansion discussed in Sec. III has been included. That is, the dynamical matrix is calculated from the energy expression using the average interplanar distances calculated in the simulation. The quasiharmonic description is seen to include most of the anharmonic effect, but part of the shift in frequency and the increase in the width of the peaks with temperature cannot be described in this way.

The variation of $\omega(T)$ and $\Delta(T)$ in Fig. 5 is approximately linear. This is true to a first approximation for all the modes studied, and in Table II we compare the slopes $\Omega_1 = d\Omega/dT$ and $\Delta_1 = d\Delta/dT$ for the three modes studied. In this table we also include the result of the

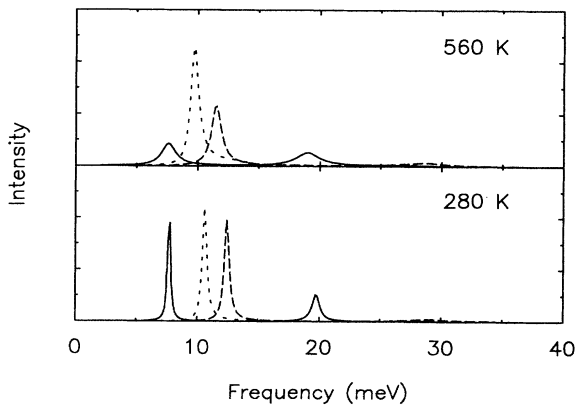

FIG. 4. The calculated density of phonon states in the three polarization directions (in-plane longitudinal is shown with a solid line, shear horizontal is short dashed, and the out-of-plane transversal is shown long dashed) for the $\bar{Y}$ zone boundary phonons in the first layer on the Cu(110) surface at 280 and 560 K.

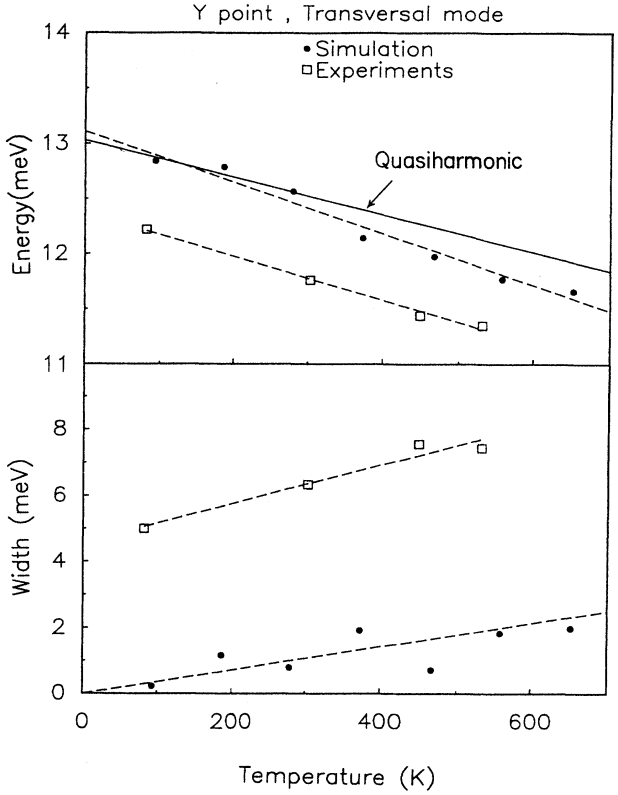

FIG. 5. The calculated frequency and width for the (S_3) $\bar{Y}$ zone boundary phonon on the Cu(110) surface. The results of the EELS experiment of Baddorf and Plummer (Ref. 4) are included for comparison. The experimental width includes a constant contribution of about 5 meV from the instrumental resolution. The dashed lines represent a linear regression through the experimental or simulated results. The solid line represents the result of a calculation using the quasiharmonic approximation.

TABLE II. The temperature derivative of the frequency (Ω_1) and width (Δ_1) of the three $\bar{Y}$ modes that are split below the bulk phonon bands on the Cu(110) surface. The frequency shift is calculated both from the simulation and in the quasiharmonic approximation (Ω_1^{qh}).

	S_1	E	S_3
Ω_1(meV/100 K)	−0.19(±0.06)	−0.27(±0.03)	−0.27(±0.02)
Ω_1^{qh}(meV/100 K)	−0.03(±0.01)	−0.16(±0.03)	−0.17(±0.03)
Δ_1(meV/100 K)	0.31(±0.10)	0.13(±0.08)	0.29(±0.12)

quasiharmonic approximation. It is seen that the quasiharmonic approximation describes the trend in Ω_1 even though the absolute magnitude is too small. The two higher-energy modes are shifting faster with increasing temperature than the lowest-energy mode. The main reason for this difference is that the two higher-energy modes are seen from Fig. 3 to be largely concentrated in the first layer, where the effect of the large thermal expansion in the first interlayer spacing is expected to be largest.

V. SURFACE ORDER

In order to study the order at the surface and the temperature effects we calculate the layer structure factor defined by

$$S_l(\mathbf{k}) = \left| \left\langle \frac{1}{N_l} \sum_{i \in l} e^{-i\mathbf{k}\cdot\mathbf{R}_i} \right\rangle \right|^2 . \quad (9)$$

$S_l(\mathbf{k})$ is a measure of the order in the nuclear positions along $\mathbf{k}$ in layer l.

In Fig. 6 we show $S_1(\mathbf{k})$ for the first layer as a function of temperature both for $\mathbf{k}$ perpendicular to the surface and for $\mathbf{k}$ having components parallel to the surface. On the semilogarithmic plot $S_1(\mathbf{k})$ is seen to fall off linearly with temperature as would be expected in a simple harmonic Debye-Waller theory. Between 500 and 600 K there is, however, a deviation from the simple linear dependence indicating an increase in the disorder. This is only observed for $\mathbf{k}$ having a component perpendicular to the surface indicating that the disorder is in this direction. The in-plane order is not changed significantly in this temperature range.

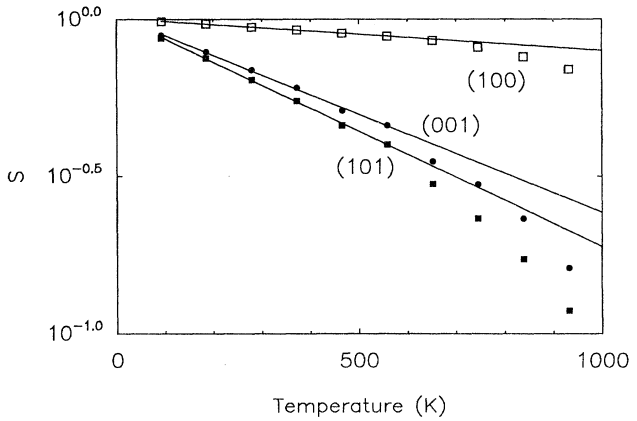

FIG. 6. The structure factor [Eq. (9)] for the first layer of a Cu(110) surface. Results are shown for $\mathbf{k}$ = (100), (001), and (101). The unit of the wave vector in the x direction is $2\pi/\sqrt{2}a$ [the (100) peak is then the first allowed Bragg reflection from the surface], whereas perpendicular to the surface it is chosen so that a (001) vector is the change of wave vector that a 30-meV He atom experiences when reflected from a surface (3.28 bohr^{-1}). This choice is made to simulate the intensity variation of a specularly scattered hyperthermal He beam.

The change in out-of-plane order around 550 K agrees nicely with the findings of both low-energy ion scattering and He scattering experiments. The change in $S_1(\mathbf{k})$ is less dramatic than in the specular He scattering experiment. This most likely is related to the fact that $S_1(\mathbf{k})$ is approximately what would be measured in a (hypothetical) neutron scattering experiment that was able to pick up a signal only from layer 1. In a He scattering experiment it is only possible to study the outermost layer, but the scattering is not directly from the nuclei. Rather, the low-energy He atoms scatter from the outermost tails of the electron distribution so the scattering with wave-vector exchange $\mathbf{k}$ is expected to be related to $S_1(\mathbf{k})$, but not identical to it. Hyperthermal He atoms are known to scatter very strongly from defects like adatoms or vacancies at the surface,[6] so it is most likely that atoms that make large excursions out from the surface due to the anharmonic potential will give rise to a much larger change in the He scattering intensity than in $S_1(\mathbf{k})$.

VI. ADATOM-VACANCY PAIR FORMATION

Apart from the enhanced anharmonicity at the surface it has also been suggested that thermal generation of adatom-vacancy pairs at the outermost surface layer might be responsible for some of the disorder at the Cu(110) surface at elevated temperatures.[5,8] In Fig. 7 we show the occupancy in various layers as a function of temperature in the simulations. It is seen that the number of adatoms starts to grow significantly around 1000 K and that the atoms mainly come from the first layer at lower temperatures whereas the vacancy formation propagates inward as the temperature increases. The rise in the number of adatoms does not seem to coincide with the drop in scattering intensity around 550 K, thus excluding this as the main cause of the intensity drop. This is in fine agreement with both the low-energy ion[8] and He scattering experiments.[6]

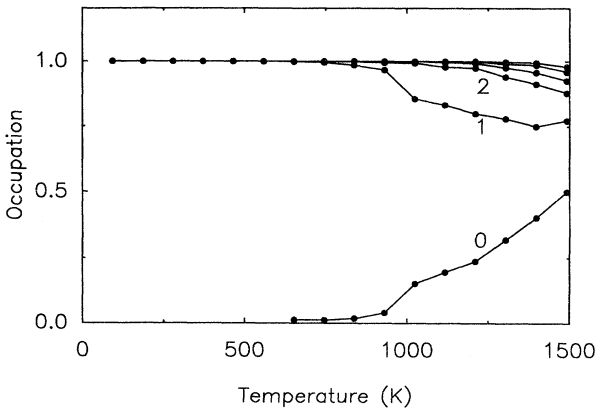

FIG. 7. The occupancy θ_l of each layer l as a function of temperature. $\theta_l = 1$ corresponds to a full layer. The adatoms are seen as a population of layer 0.

Figure 8 shows an Arrhenius plot of the adatom concentration. We only include the high-temperature points where we have good statistics in the plot. From the slope of the figure we deduce an activation energy for adatom formation of 0.35 eV in reasonable agreement with the value of 0.2 eV deduced from the low-energy scattering experiment.[8] He scattering experiments have indicated the existence of an activation energy of 0.27 eV (Ref. 5) for the creation of some defect on the Cu(110) surface, but here the exact nature of the defect was not specified.

There is an interesting aspect about the activation energy for adatom formation that needs to be discussed further. If one calculates the energy of taking an atom from the first layer and placing it away from the range of the vacancy that is left behind, one finds that the energy for this process is as high as 0.6 eV.[19] The much smaller energy deduced from the simulation arises due to adatom-adatom and vacancy-vacancy interactions. Figure 9 shows a snapshot of the atomic configurations at 1025 K. It is clearly seen how the adatoms and the vacancies have a tendency to cluster together. Two adatoms

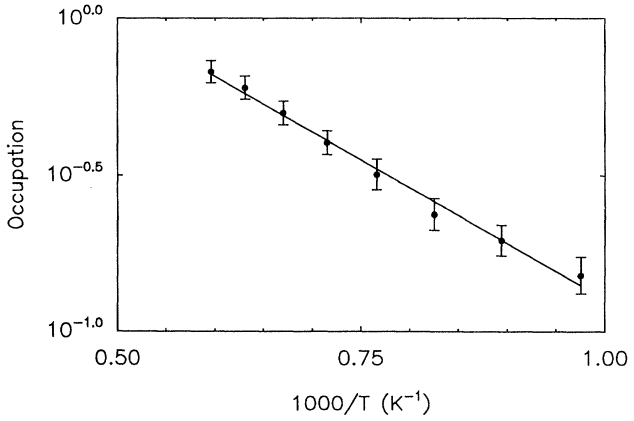

FIG. 8. An Arrhenius plot of the adatom concentration on Cu(110).

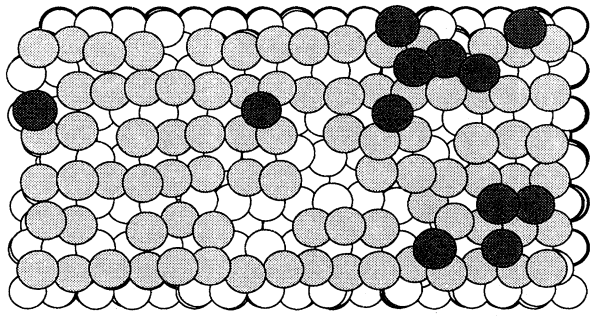

FIG. 9. A snapshot of the atomic configurations of a Cu(110) surface at 1025 K. The adatoms are the darkest, the first layer atoms somewhat lighter, and the deeper layer atoms are white.

or two vacancies at nearest-neighbor sites are bound together by 0.15 eV per atom (or vacancy). In the simulation there is therefore a considerable concentration of such "bonds" and the effective adatom formation energy is considerably smaller than the single adatom value. We expect that the same holds for the experimentally deduced values.

VII. PREMELTING

The behavior of the structure factor at higher temperatures can be seen in Fig. 10. Around 1000 K the order starts to decrease drastically, and the decrease is also observed for the in-plane structure factor. Further-

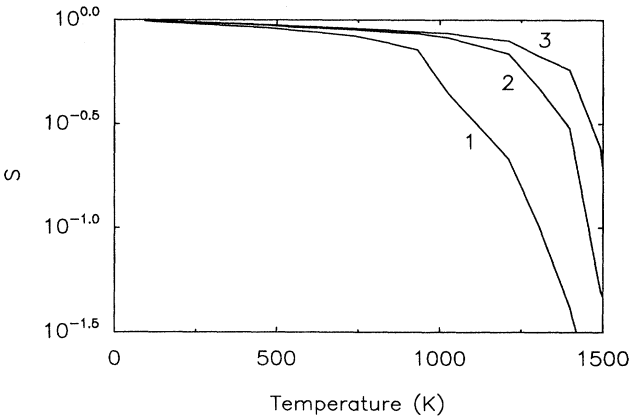

FIG. 10. The structure factor [Eq. (9)] for the three outermost layers of a Cu(110) surface. Results are shown for $\mathbf{k} = (100)$. The layer by layer disordering typical of premelting is observed. Due to the static substrate below layer 8 the disordering temperature does not approach the bulk melting point for the deeper layers. This means that we cannot determine a good value for the melting point. Taking into account that there are only eight dynamical layers on top of the static substrate, we anticipate a melting temperature in the range 1400–1500 K for this potential in reasonable agreement with the experimental melting point for Cu of 1356 K (Ref. 24).

more, the layers are seen to lose the order one by one, starting with the outermost one. This behavior has been observed experimentally for Pb(110) (Ref. 3) and Al(110) (Ref. 20) and is known as premelting. Simulations using the effective-medium theory have been able to describe this in great detail for Al(110).[21–23,20] The present results are not qualitatively different.

As for the Al(110) surface, one can see by comparing the temperature dependence of the adatom-vacancy formation (Fig. 7) with the temperature dependence of the order parameter (Fig. 10) that the two effects are correlated. The loss of order can be thought of as originating from distortions of the atomic positions around the vacancies and the adatoms. These distortions are clearly observable in Fig. 9.

VIII. CONCLUSIONS

We have presented the results of a molecular-dynamics simulation of the finite-temperature properties of a Cu(110) surface. A complete picture of the dynamical properties of the surface from room temperature to the melting point emerges in good agreement with available experimental observations. The thermal expansion of the first interlayer spacings is considerably larger than in the bulk. We find large anharmonic shifts in phonon frequencies and an increase in the width of the peaks in the phonon density of states with temperature which is again considerably larger than in the bulk. The order in the first layer as measured by the structure factor shows three regimes. At low temperature the order decreases in an ordinary Debye-Waller fashion indicating that a harmonic description is essentially valid for the structure factor although the mentioned changes in the vibration spectrum indicate that some anharmonicity is present in the system. Above 550 K there is an additional decrease in the out-of-plane order, which can be described to an increased influence of anharmonicity for motion perpendicular to the surface. Above 1000 K the in-plane order starts to decrease faster than expected from a Debye-Waller description. The loss of order is shown to coincide with an onset in the formation of adatom-vacancy pairs at the surface. The loss of in-plane order is associated with relaxations of the atoms surrounding the adatoms and vacancies. As the melting point is approached the vacancy formation penetrates to the deeper layers. This is accompanied by a gradual layer-by-layer loss of order, known as premelting.

ACKNOWLEDGMENTS

Many discussions with K. W. Jacobsen are gratefully acknowledged. Financial support has been provided by the Danish Research Councils through the Center for Surface Reactivity.

APPENDIX

In this appendix we will show that in the harmonic approximation the correlation function $n_l^\alpha(\mathbf{k},\omega)$ defined in Eqs. (2)–(4) is identical to the projected phonon density of states in layer l and direction α, which is defined as

$$\rho_l^\alpha(\mathbf{k},\omega)=\sum_\sigma |\varepsilon_{l,\mathbf{k}\sigma}^\alpha|^2\delta(\omega-\omega_{\mathbf{k}\sigma}). \tag{A1}$$

Here $\varepsilon_{l,\mathbf{k}\sigma}^\alpha$ is the eigenvector in layer l corresponding to the eigenfrequency $\omega_{\mathbf{k}\sigma}$.

Within the harmonic approximation the phonons are plane waves parallel to the surface, and the momentum autocorrelation function can be expressed in terms of the phonon coordinates. The reciprocal surface representation of the momentum in layer l is defined by

$$p_{l,\mathbf{k}}^\alpha(t)=\frac{1}{N_l}\sum_{i\in l} p_i^\alpha(t)e^{-i\mathbf{k}\cdot\mathbf{R}_i}, \tag{A2}$$

where $\mathbf{k}$ is the surface crystal momentum and $\mathbf{R}_i$ is the two-dimensional projection of the equilibrium atomic coordinate onto the surface. However, for convenience we will not distinguish between two- and three-dimensional vectors, so that the surface crystal momentum is just defined as a three-dimensional momentum with 0 as the third component and $\mathbf{R}_i$ is the full three-dimensional coordinate of atom i. The momentum $p_{i\in l}^\alpha(t)$ is expanded in surface phonon coordinates:

$$\begin{aligned} p_{i\in l}^\alpha(t)&=\frac{-i}{\sqrt{N}}\sum_{\mathbf{k},\sigma}\left(\frac{M\omega_{\mathbf{k}\sigma}}{2}\right)^{1/2}(a_{\mathbf{k}\sigma}-a_{-\mathbf{k}\sigma}^*)\\ &\quad\times\varepsilon_{l,\mathbf{k}\sigma}^\alpha e^{i\mathbf{k}\cdot\mathbf{R}_i-i\omega_{\mathbf{k}\sigma}t}\\ &=\frac{M}{\sqrt{N}}\sum_{\mathbf{k},\sigma}\dot{Q}_{\mathbf{k}\sigma}(t)\varepsilon_{l,\mathbf{k}\sigma}^\alpha e^{i\mathbf{k}\cdot\mathbf{R}_i}, \end{aligned} \tag{A3}$$

where $Q_{\mathbf{k}\sigma}(t)=(a_{\mathbf{k}\sigma}+a_{-\mathbf{k}\sigma}^*)e^{-i\omega_{\mathbf{k}\sigma}t}/\sqrt{2\omega_{\mathbf{k}\sigma}}$ is the classical amplitude and N is the total number of atoms. Then the momentum autocorrelation function is expanded in phonon coordinates:

$$\begin{aligned} \frac{1}{2M}\langle p_{l,\mathbf{k}}^\alpha(t)p_{l,\mathbf{k}}^\beta(0)\rangle&=\frac{1}{N_l^2}\sum_{i,j\in l}e^{-i\mathbf{k}\cdot(\mathbf{R}_i-\mathbf{R}_j)}\frac{1}{2M}\langle p_i^\alpha(t)p_j^\beta(0)\rangle\\ &=\sum_{\mathbf{k}',\sigma',\mathbf{k}'',\sigma''}\frac{1}{NN_l^2}\sum_{i,j\in l}e^{-i(\mathbf{k}-\mathbf{k}')\cdot(\mathbf{R}_i-\mathbf{R}_j)}e^{-i(\mathbf{k}'-\mathbf{k}'')\cdot\mathbf{R}_j}\frac{M}{2}\varepsilon_{l,\mathbf{k}'\sigma'}^\alpha\varepsilon_{l,\mathbf{k}''\sigma''}^{\beta*}\langle\dot{Q}_{\mathbf{k}'\sigma'}(t)\dot{Q}_{\mathbf{k}''\sigma''}^*(0)\rangle\\ &=\frac{1}{N}\sum_\sigma\frac{M}{2}\langle\dot{Q}_{\mathbf{k}\sigma}(0)\rangle^2\varepsilon_{l,\mathbf{k}\sigma}^\alpha\varepsilon_{l,\mathbf{k}\sigma}^{\beta*}e^{i\omega_{\mathbf{k}\sigma}t}\\ &=\frac{\frac{1}{2}kT}{N}\sum_\sigma\varepsilon_{l,\mathbf{k}\sigma}^\alpha\varepsilon_{l,\mathbf{k}\sigma}^{\beta*}e^{i\omega_{\mathbf{k}\sigma}t}. \end{aligned} \tag{A4}$$

Here we have used the facts that $Q_{\mathbf{k}\sigma}(t) = Q_{\mathbf{k}\sigma}(0)e^{-i\omega_{\mathbf{k}\sigma}t}$ and that the average energy of a single harmonic oscillator is given by $\langle E\rangle = \frac{1}{2}M\langle\dot{Q}\rangle^2 = \frac{1}{2}kT$ due to the equipartition of energy in the phonon degrees of freedom. The polarization vectors are normalized such that $\sum_{l,\alpha}|\epsilon^{\alpha}_{l,\mathbf{k}\sigma}|^2 = 1$ and we get similarly

$$\frac{1}{2M}\sum_{l,\alpha}\langle p^{\alpha}_{l,\mathbf{k}}(0)p^{\alpha}_{l,\mathbf{k}}(0)\rangle = \frac{1}{N}\sum_{\sigma}\tfrac{1}{2}kT = \frac{\frac{3}{2}kT}{N_l}, \tag{A5}$$

since $\sum_{\sigma}1 = 3N/N_l = 3N_{\text{layer}}$, where N_{layer} is the number of layers.

The correlation function $n^{\alpha}_l(\mathbf{k},\omega)$ in Eq. (2) can then be obtained from Eq. (A5) and the Fourier transform $\mathcal{F}$ of (A4) as

$$n^{\alpha}_l(\mathbf{k},\omega) = \frac{\mathcal{F}(\langle p^{\alpha}_{l,\mathbf{k}}(t)p^{\alpha}_{l,\mathbf{k}}(0)\rangle)}{\sum_{m,\beta}\langle p^{\beta}_{m,\mathbf{k}}(0)p^{\beta}_{m,\mathbf{k}}(0)\rangle/3N_{\text{layer}}} = \sum_{\sigma}|\epsilon^{\alpha}_{l,\mathbf{k}\sigma}|^2\delta(\omega-\omega_{\mathbf{k}\sigma}), \tag{A6}$$

which is exactly the density of states defined in Eq. (A1).

In the general case, including the anharmonicity, it is important to take into account the thermal expansion that is not included in the harmonic approximation. In the calculation, see Eq.(4), we have used the instantaneous atomic positions rather than the harmonic equilibrium positions. When using the instantaneous atomic positions, at low temperature, this will result in a Debye-Waller-like contribution and a small contribution from the multiphonon expansion, both of which will always be present in an experiment measuring the phonon density of states.

[1] J. W. M. Frenken, F. Huussen, and J. F. van der Veen, Phys. Rev. Lett. **58**, 401 (1987).

[2] K. S. Liang, E. B. Sirota, K. L. D'Amico, G. J. Hughes, and S. K. Sinha, Phys. Rev. Lett. **59**, 304 (1987); E. H. Conrad, R. M. Aten, D. S. Kaufman, L. R. Allen, and T. Engel, J. Chem. Phys. **84**, 1015 (1986); F. Fabre, B. Salanon, and J. Lapujoulade, in *The Structure of Surfaces II*, edited by J. F. van der Veen and M. A. van Hove (Springer, Berlin, 1988), p. 520.

[3] J. W. M. Frenken, P. M. J. Maree, and J. F. van der Veen, Phys. Rev. Lett. **59**, 2678 (1987); K. Prince, U. Breuer, and H. P. Bonzel, *ibid.* **60**, 1146 (1988).

[4] A. P. Baddorf and E. W. Plummer, J. Electron Spectrosc. **54/55**, 541 (1990).

[5] D. Gorse and J. Lapujoulade, Surf. Sci. **162**, 847 (1987).

[6] P. Zeppenfeld, K. Kern, R. David, and G. Comsa, Phys. Rev. Lett. **62**, 63 (1989).

[7] R. S. Williams, P. S. Wehner, J. Stöhr, and D. A. Shirley, Phys. Rev. Lett. **39**, 302 (1977).

[8] Th. Fauster, R. Schneider, H. Dürr, G. Engelmann, and E. Taglauer, Surf. Sci. **189/190**, 610 (1987).

[9] S. G. J. Mochrie, Phys. Rev. Lett. **59**, 304 (1987).

[10] C. S. Jayanthi, E. Tosatti, and L. Pietronero, Phys. Rev. B **31**, 3456 (1985).

[11] J. K. Nørskov and K. W. Jacobsen, in *The Structure of Surfaces II*, edited by M. van Hove and F. van der Veen, Springer Series in Surface Science (Springer, Berlin, 1987), Vol. 11, p. 118.

[12] K. W. Jacobsen and J. K. Nørskov, Phys. Rev. Lett. **59**, 2764 (1987); **60**, 2496 (1988); **65**, 1788 (1990).

[13] P. Ditlevsen and J. K. Nørskov, Surf. Sci. **254**, 261 (1991).

[14] K. W. Jacobsen, J. K. Nørskov, and M. J. Puska, Phys. Rev. B **35**, 7423 (1987); K. W. Jacobsen, Comments Cond. Mat. Phys. **14**, 129 (1988).

[15] W. B. Pearson, *A Handbook of Lattice Spacings and Structures of Metals and Alloys* (Pergamon, New York, 1958).

[16] J. M. Dickey and A. Paskin, Phys. Rev. **188**, 1407 (1969).

[17] W. H. Press, B. P. Flannery, S. A. Teukolsky, and W. T. Vetterling, *Numerical Recipes in C* (Cambridge University Press, Cambridge, 1988), Sec. 12.8.

[18] P. Zeppenfeld, K. Kern, R. David, K. Kuhnke, and G. Comsa, Phys. Rev. B **38**, 12 329 (1988).

[19] K. W. Jacobsen and P. Stoltze, in *Ordering at Surfaces and Interfaces*, edited by A. Yoshimori, T. Shinjo, and M. Watanabe (Springer, Berlin, 1991).

[20] A. W. Denier van der Gon, D. Frenkel, J. W. M. Frenken, R. Smith, and P. Stoltze, Surf. Sci. **256**, 385 (1991).

[21] P. Stoltze, J. K. Nørskov, and U. Landman, Phys. Rev. Lett. **61**, 440 (1988).

[22] P. Stoltze, J. K. Nørskov, and U. Landman, Surf. Sci. **220**, L693 (1989).

[23] P. Stoltze, J. Chem. Phys. **92**, 6306 (1990).

[24] N. W. Ashcroft and N. D. Mermin, *Solid State Physics* (Holt, Reinhart, and Winston, New York, 1976).

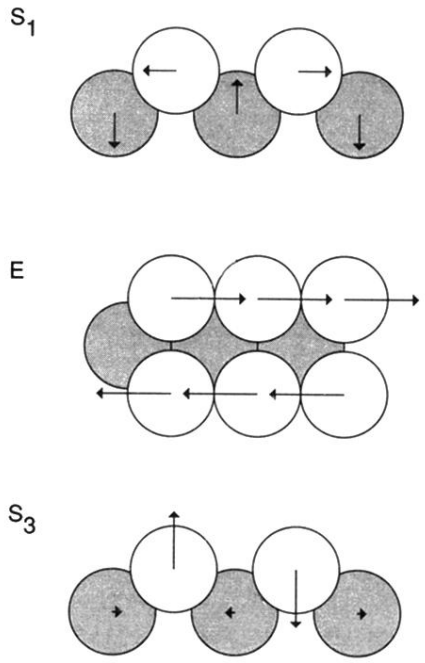

FIG. 3. Schematic illustration of the motion of the two outermost layers for the three $\bar{Y}$ zone boundary phonons on the Cu(110) surface. The polarizations in different directions and in the first few layers as calculated in the harmonic approximation are indicated by the lengths of the vectors shown.